

# Optimization for Micro-energy Grid Dispatch Based on Non-supplementary Fired Compressed Air Energy Storage Aided Energy Hub and Hybrid Hyper-spherical Search

Zhenlong Li, Peng Li, Jing Xia, and Xiangqian Liu

**Abstract**—Micro-energy grids have shown superiorities over traditional electricity and heating management systems. This paper presents a hybrid optimization strategy for micro-energy grid dispatch with three salient features. First, to enhance the ability to support new storage equipment, an energy hub model is proposed using the non-supplementary fired compressed air energy storage (NSF-CAES). This provides flexible dispatch for cooling, heating and electricity. Second, considering the unique characteristics of the NSF-CAES, a sliding time window (STW) method is designed for simple but effective energy dispatch. Third, for the optimization of energy dispatch, we blend the differential evolution (DE) with the hyper-spherical search (HSS) to formulate a hybrid DE-HSS algorithm, which enhances the global search ability and accuracy. Comparative case studies are performed using real data of scenarios to demonstrate the superiorities of the proposed scheme.

**Index Terms**—Energy hub dispatch, hyper-spherical search, micro-energy grid, sliding time window.

## I. INTRODUCTION

THERE have been wide explorations on the use of clean energies such as wind and solar energy for sustainable development. The concept of microgrid based on distributed power generation technologies is proposed. The micro-energy grid is formulated as a new microgrid architecture which integrates multiple energy carriers such as cooling, heating, and electricity [1]. This architecture requires the coordination of the natural gas network and the power network.

Manuscript received: August 27, 2020; revised: January 26, 2021; accepted: May 17, 2021; Date of CrossCheck: May 17, 2021. Date of online publication: July 28, 2021.

This work was supported by the Fundamental Research Funds for the Central Universities (No. 2019JBM004), the National Natural Science Foundation of China (No. 51977004), and the Beijing Natural Science Foundation (No. 4212042).

This article is distributed under the terms of the Creative Commons Attribution 4.0 International License (<http://creativecommons.org/licenses/by/4.0/>).

Z. Li, P. Li, and X. Liu (corresponding author) are with Beijing Jiaotong University, Beijing, China (e-mail: BJTU\_LZL@bjtu.edu.cn; lipeng@bjtu.edu.cn; xqliu@bjtu.edu.cn).

J. Xia is with State Key Laboratory of Alternate Electrical Power System with Renewable Energy Sources, North China Electric Power University, Beijing, China, and she is also with Beijing Goldwind Science & Creation Wind Power Equipment Co., Ltd., Beijing, China (e-mail: xiajinghit@126.com).

DOI: 10.35833/MPCE.2020.000639

Thus, the combined heating and power (CHP) technology plays an important role in coupling the natural gas system and the power system.

For the micro-energy grid containing multiple energy carriers, some studies adopt a system framework called energy hub for system analysis [2]. The energy hub adopts the CHP and combines the energy storage with other energy conversion equipments. It provides high flexibility for the coordinated dispatch of various forms of carriers such as cold, heating and electricity [3]. Despite various applications of the energy hub, there still exist some problems in system modeling and optimization solving.

For the modeling of micro-energy grid system with energy hubs, the utility as well as the modeling and use of new devices for energy hubs should be considered. In [4], a model is presented for economic dispatch of multi-energy grid systems using energy hubs. In [5], a residential energy hub model is proposed with a demand response program for the optimal energy management. Some studies improve the energy hub in the presence of uncertainties using searching algorithms [6]–[8]. In [9], the day-ahead and real-time energy management models are established and formulated as a class of distributed coupled optimization problems.

Obviously, these studies provide improved micro-energy grid system models but some new issues need to be considered for further applications. For example, the vehicle to grid is effective to deal with flexible heating load, but the model is too complicated for the solvers [4], [5]. New equipments like heating pump water heater and hydrogen storage can enhance the energy hub, but they require simplified dispatch model or reduced objectives for optimization [6], [8], [9]. Recent studies use the compressed air energy storage (CAES) equipment in power system dispatch. The CAES provides not only electrical energy, but also other carrier forms of energies such as cooling and heating. It also uses natural gas combustion to generate electricity and causes environmental problems similar to CHP. The advanced adiabatic CAES (AA-CAES) system and the non-supplementary combustion CAES (NSF-CAES) system integrate the thermal energy storage system into CAES [10]. They can store the heating generated in the air compression process and re-

lease it to heat the compressed air during the power generation process. Thus, no gas combustion is required in the CAES system. In [11], the normal CAES with gas supply is introduced to reduce the system operating cost and uncertainty influence of wind power. In [12], the adiabatic CAES is used as back-up power to support microgrid operation. In [13], an energy hub based on adiabatic CAES is proposed by considering the pressure behavior and mass flow changes. In [10], the micro-energy grid dispatch is addressed by using the NSF-CAES to absorb electricity and release cooling, heating and electricity. The NSF-CAES can be dispatched independently for more practical applications. In this paper, considering the need for zero carbon emissions and the characteristics of the energy hub based micro-energy grid system, we introduce an NSF-CAES equipment to improve the energy hub model.

For the dispatch of micro-energy grid system, there have been many methods such as dynamic programming, game theory, intelligent algorithms, etc. [14]. Generally, these methods can be categorized into two types: analytical methods and numerical methods. Analytical methods are limited and used for some unique scenarios. Numerical methods can be applied more widely owing to the strong searching ability and less limitations on system model [15]. Thus, numerical methods can effectively address typical linear programming and convex optimization issues. They can also solve multi-objective and non-linear problems conveniently. Moreover, numerical methods show better generalization performance for various scenarios, with straightforward logic flow for algorithm realization.

In this paper, we survey the two types of methods, respectively. For analytical methods, a three-level framework has been used to optimize the microgrid with stochastic programming for uncertainties [16]. A priority-based energy dispatch method for distributed networks is presented for multiple microgrids [17]. A two-layer predictive energy management system is formulated with hybrid storages [18]. A multi-stage stochastic programming of a transmission constrained economic dispatch is provided subject to multi-area renewable production uncertainty [19].

In comparison, numerical methods focus more on intelligent algorithms. Some multi-objective energy management methods for microgrids use bio-inspired mechanisms like imperialistic competition algorithm (ICA) and Levy-harmony algorithm to prevent premature convergence [20], [21]. The trade-off between the searching speed and precision is a vital issue determined by seeking mechanisms. Therefore, some improved intelligent algorithms have been raised [22]. Besides, if the objective function or constraints cannot be directly achieved, data-driven and robust algorithms are preferable [23], [24].

Most analytical methods rely on convex optimization, thus the solutions to non-convex optimization need further study. Intelligent algorithms can make trade-off between the searching speed and precision, but tackling scenarios with too many constrains will lead to non-convergence. Recently, it is found that the hyper-spherical search (HSS) algorithm performs well in micro-energy grid dispatch optimization, but

there exists the probability of falling into the local optimal due to the searching limitation [7], [25].

Inspired by the above observations, we propose an energy hub framework by introducing the NSF-CAES. Then, a dispatch scheme is designed with the differential evolution aided HSS (DE-HSS) algorithm. The major contributions of this work are two-fold.

1) The NSF-CAES is involved in the energy hub, providing flexible support for storage devices. Note that the NSF-CAES needs to compress air during the energy storage process. This cannot ensure real-time dispatch. Therefore, we adopt a sliding time window (STW) method for effective energy dispatch and service life extension of the NSF-CAES.

2) To optimize the complex micro-energy grid, the DE-HSS algorithm is presented for the energy dispatch. Compared with traditional intelligent optimization methods, the DE-HSS has stronger searching ability and avoids the deficits of long-time computation, low precision and local optima.

The rest of the paper is organized as follows. Section II describes the framework and modeling for micro-energy grid. Section III presents the formulation of multi-objective optimization. Section IV presents the dispatch method using STW and DE-HSS. Case studies and comparative analysis are carried out in Section V to validate the proposed methods. Finally, the concluding remarks are given in Section VI.

## II. FRAMEWORK AND MODELING FOR MICRO-ENERGY GRID

### A. Framework of Micro-energy Grid and Solution Process

This paper studies the community-scale micro-energy grid. The first step to solve the micro-energy grid dispatch problem is to build a model. Then an algorithm is used to solve it according to the given model and data. Thus we divide the overall calculation process into two layers: the micro-energy grid layer and the dispatch layer.

The framework of micro-energy grid is shown in Fig. 1. The gas company serves as energy supplier while the electricity company serves as energy supplier or receiver. The energy hub acts as a multi-energy aggregator, which is composed of wind turbines, solar panels, CHP equipment, electric boiler (EB), gas boiler (GB), absorption chiller (AC), electric storage (ES), heating storage (HS), and NSF-CAES.

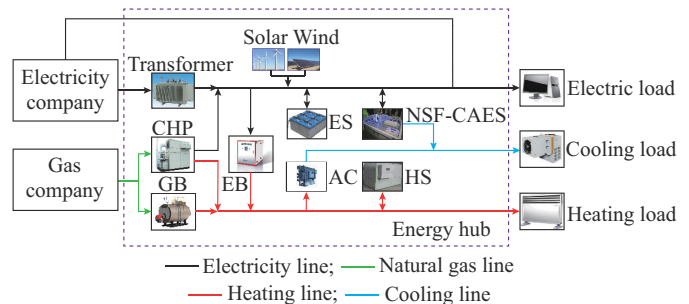


Fig. 1. Framework of micro-energy grid.

It is assumed that the communication lines and all equipments are in normal status. On the input side, the electricity company provides the electricity to energy hub via trans-

formers. The gas company provides the gas to CHP and GB with dispatch factor adaptively tuned by demand and equipment constraints. Inside the energy hub, the electric power comes from solar, wind, and electricity output of CHP. The heating power comes from EB, GB, and the heating output of CHP. The cooling power comes from AC. Storage devices balance the supply and demand. Electricity load, cooling load, and heating load are different loads on the output side.

Figure 2 shows the framework of micro-energy grid dispatch.

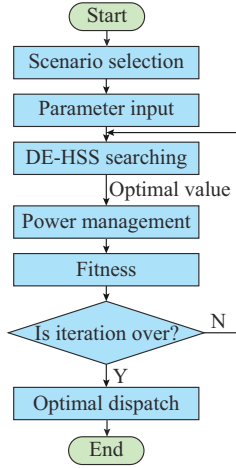


Fig. 2. Framework of micro-energy grid dispatch.

In this paper, the system advisor model (SAM) is used to simulate wind and solar power without mathematical modeling [26]. Three scenarios are studied: environmental cost minimization, economic cost minimization, and environmental and economic cost minimization. For each scenario, the proposed DE-HSS seeks the optimal value for power management.

## B. System Modeling

### 1) CHP Modeling

The CHP is composed of a micro gas turbine and a bromine refrigerator [6]. We investigate a CHP in the normally open state without consideration of the start and stop time. The CHP determines the electric energy output by the thermal energy output. It is modeled as:

$$\begin{cases} \eta_{MT} = a \left( \frac{P_t^{MT}}{P_{MT}} \right)^3 - b \left( \frac{P_t^{MT}}{P_{MT}} \right)^2 + c \left( \frac{P_t^{MT}}{P_{MT}} \right) + d \\ Q_t^{MT} = \frac{(1 - \eta_{MT} - \eta_l) P_t^{MT}}{\eta_{MT}} \\ P_{h,t}^{CHP} = \eta_h Q_t^{MT} \\ P_t^{CHP} = \frac{P_t^{MT}}{\eta_{MT}} \end{cases} \quad (1)$$

where  $\eta_{MT}$  is the electricity generation efficiency of micro gas turbine;  $P_t^{MT}$  is the electricity output of micro gas turbine at time  $t$ ;  $P_{MT}$  is the rated power of micro gas turbine;  $a$ ,  $b$ ,  $c$ , and  $d$  are the fitting coefficients and set to be 0.0753, 0.3095, 0.4174, and 0.1068, respectively [27];  $Q_t^{MT}$  is the re-

sidual heating at time  $t$ ;  $\eta_l$  is the heating loss coefficient;  $\eta_h$  is the heating generation efficiency;  $P_{h,t}^{CHP}$  is the actual heating production from the residual heating at time  $t$ ; and  $P_t^{CHP}$  is the power corresponding to the natural gas consumed at time  $t$ .

### 2) Dispatch Factor Between CHP and GB

Natural gas is consumed through CHP and GB. The distribution formulations of natural gas between CHP and GB are:

$$\begin{cases} P_t^{CHP} = v_g P_t^{gas} \\ P_t^{GB} = (1 - v_g) P_t^{gas} \end{cases} \quad (2)$$

where  $P_t^{gas}$  is the natural gas consumption at time  $t$ ; and  $v_g$  is the dispatch factor of natural gas which is adaptively tuned in different time intervals.

### 3) ES and HS Modeling

Due to the similarity of models, the ES and HS can be mathematically described with the same model [5] given as:

$$E_t = (1 - \eta^{loss}) E_{t-1} + \eta^{ch} P^{ch} \Delta t - \frac{P^{dis} \Delta t}{\eta^{dis}} \quad (3)$$

where  $\Delta t$  is the time length;  $\eta^{ch}$  and  $\eta^{dis}$  are the charging and discharging efficiencies, respectively;  $p^{ch}$  and  $p^{dis}$  are the charging and discharging power, respectively;  $\eta^{loss}$  is the self-loss rate; and  $E$  is the quantity of energy storage.

### 4) EB, GB, and AC Modeling

The EB cooperates with CHP to meet the heating load demand and increase the electricity consumption during the valley periods [28]. It enables the conversion from the electricity to heating as well as peak-valley coordination between electricity load and heating load, which can be modeled as:

$$\tilde{P}_t^{EB} = \eta_h^{EB} P_t^{EB} \quad (4)$$

where  $P_t^{EB}$  and  $\tilde{P}_t^{EB}$  are the electric and heating power of the EB at time  $t$ , respectively; and  $\eta_h^{EB}$  is the conversion efficiency from electricity to heating. In this paper, the electric energy consumed by the EB is uniformly dispatched as part of the electricity load for the micro-energy grid.

The heating power generated by the GB is related to the efficiency:

$$\tilde{P}_t^{GB} = \eta_h^{GB} P_t^{GB} \quad (5)$$

where  $\tilde{P}_t^{GB}$  is the heating output of the GB at time  $t$ ; and  $\eta_h^{GB}$  is the model efficiency of the GB.

The AC converts the heating power into cooling power:

$$\tilde{P}_t^{AC} = \eta_e^{AC} P_t^{AC} \quad (6)$$

where  $\tilde{P}_t^{AC}$  is the cooling output of the AC at time  $t$ ;  $P_t^{AC}$  is the consumed heating power of the AC at time  $t$ ; and  $\eta_e^{AC}$  is the cooling efficiency of the AC.

### 5) NSF-CAES Modeling

We model the NSF-CAES in two ways: ① component-level modeling; ② STW-based system-level modeling.

#### 1) Component-level modeling

The NSF-CAES used in this paper is mainly composed of a compressor, a motor/generator, a turbine generator, a gas storage chamber, a high-temperature medium storage tank, a low-temperature medium storage tank, and heating exchangers. It operates in two processes: energy storage and energy

release. Figure 3 describes the framework of NSF-CAES, where  $P_i$  ( $i=0, 1, \dots, 8$ ) is the corresponding power entering or exiting each energy conversion sub-equipment of NSF-CAES and  $T_i$  ( $i=0, 1, \dots, 8$ ) is the temperature of the air before entering the heating exchanger or after exiting from the heating exchanger. More specific assumptions for NSF-CAES can be found in [10]. Here we assume that both the compressor and the turbine generator use the rated voltage during the operation, and the specific parameters are given in Section V.

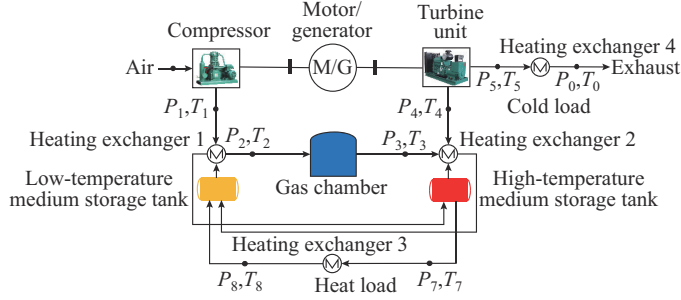


Fig. 3. Framework of NSF-CAES.

The mathematical model for the NSF-CAES at runtime is given as follows.

a) Electricity consumed by energy storage. The compressor can use wind power, solar power, and valley power to compress air. The shaft power at each compression stage is:

$$P_{c,i} = \frac{k}{k-1} \frac{Q_{m,c} R_g T_{c,i}^{in}}{\eta_{c,i}} \beta_{c,i}^{\frac{k-1}{k}} \quad (7)$$

where  $k$  is the adiabatic index;  $Q_{m,c}$  is the mass flow rate of the compressor;  $R_g$  is the constant of the air;  $T_{c,i}^{in}$  is the temperature of the air entering into the  $i^{\text{th}}$  stage compressor;  $\eta_{c,i}$  is the efficiency of the  $i^{\text{th}}$ -stage compressor; and  $\beta_{c,i}$  is the compression ratio of the  $i^{\text{th}}$ -stage compressor.

The temperature of the air exiting into the  $i^{\text{th}}$  stage compressor  $T_{c,i}^{out}$  is:

$$T_{c,i}^{out} = T_{c,i}^{in} \frac{\beta_{c,i}^{\frac{k-1}{k}} - 1}{\eta_{c,i}} + 1 \quad (8)$$

The number of compressor stages is 3, and the time of the system energy storage process is  $t_c$ . The electric energy consumed by the compressor unit in the energy storage process is:

$$W_c = \sum_{i=1}^3 P_{c,i} t_c \quad (9)$$

b) Heat stored by the heating recovery system. The low-temperature medium in the regenerative system absorbs the compression heating in the compression process through the heating exchanger 1, and then stores it in the high-temperature medium storage tank. The heating stored in the regenerative system is the heating released by the high-pressure and high-temperature air passing through the heating exchanger 1:

$$Q_{TES} = \sum_{i=1}^3 \tau_c Q_{m,c} C_{p,a} (T_1 - T_2) \quad (10)$$

where  $C_{p,a}$  is the specific heating capacity of the air at a constant pressure; and  $\tau_c$  is the compressor working hours.

c) Electrical energy output by the system. By using the adiabatic efficiency of the turbine, the output shaft power at each stage of the turbine unit is calculated as:

$$P_{e,i} = \frac{k}{k-1} Q_{m,e} R_g T_{e,i} \eta_{e,i} \left( 1 - \pi_{e,i}^{-\frac{k-1}{k}} \right) \quad (11)$$

where  $Q_{m,e}$  is the mass flow rate of the turbine;  $T_{e,i}$  is the temperature of the air entering the  $i^{\text{th}}$ -level turbine during the expansion process;  $\eta_{e,i}$  is the efficiency of the  $i^{\text{th}}$ -level turbine; and  $\pi_{e,i}$  is the expansion ratio in the  $i^{\text{th}}$ -level turbine.

The number of the turbine stages is 2, and the actual output power of the entire turbine:

$$E_e = \eta_g \sum_{i=1}^2 P_{e,i} t_e \quad (12)$$

where  $\eta_g$  is the efficiency of the turbine; and  $t_e$  is the generation time of turbine power.

d) Heat output by system. The heating output by the system is the heating released by the high-temperature medium storage tank through the heating exchanger 3. The heating can be stored and used during discharging. The heating output is:

$$E_h = X Q_{TES} \quad (13)$$

where  $X$  is the heating ratio for the heating stored in the regenerative system.

e) Cold output by system. The cooling output of the system is the amount of heating exchange between the low-temperature exhaust of the turbine unit and the outside through the heating exchanger 4. It is assumed that the temperature of the low-temperature exhaust reaches the ambient temperature  $T_0$  after heating exchange. The cooling output is:

$$E_c = t_e Q_{m,e} C_{p,a} (T_0 - T_5) \quad (14)$$

## 2) STW-based system-level modeling

By ignoring the operation details, we consider the charging and discharging characteristics under the rated operating condition. The NSF-CAES stores the energy just as typical storage devices, and discharges the energy to the electricity load, cooling load, and heating load in different proportions. The charging model is:

$$E_{com,t} = (1 - \eta_{com}^{loss}) E_{com,t-1} + \eta_{com}^{ch} P_{com,t}^{ch} \Delta t \quad (15)$$

The discharge to electricity load, cooling load, and heating load is modeled as:

$$\begin{cases} E_{com,t} = (1 - \eta_{com}^{loss}) E_{com,t-1} - \frac{P_{com,t}^{dis} \Delta t}{\eta_{com}^{dis}} \\ E_{com,e,t}^{dis} = \eta_{com}^{com} E_{com,t} \\ E_{com,c,t}^{dis} = \eta_{com}^{com} E_{com,t} \\ E_{com,h,t}^{dis} = \eta_{com}^{com} E_{com,t} \\ \eta_{com}^{com} + \eta_{com}^{com} + \eta_{com}^{com} < 1 \end{cases} \quad (16)$$

where  $\eta_{com}^{loss}$  is the self-loss rate of NSF-CAES;  $P_{com,t}^{ch}$  and  $P_{com,t}^{dis}$  are the charging and discharging power at time  $t$ , respectively;  $\eta_{com}^{ch}$  and  $\eta_{com}^{dis}$  are the charging and discharging efficiencies, respectively;  $E_{com,e,t}^{dis}$ ,  $E_{com,c,t}^{dis}$  and  $E_{com,h,t}^{dis}$  are the energies that can be released to electric load, cooling load, and heating load at time  $t$ , respectively; and  $\eta_{com}^{com}$ ,  $\eta_{com}^{com}$ , and  $\eta_{com}^{com}$  are

the ratios of energy discharging to electricity, heating, and cooling, respectively. Due to the energy loss, there exists  $\eta_e^{com} + \eta_h^{com} + \eta_c^{com} < 1$ .

### III. FORMULATION OF MULTI-OBJECTIVE OPTIMIZATION

#### A. Multi-objective Function

##### 1) Economic Cost

It is assumed that there is no loss of energy during the transmission. We focus on the dispatch optimization for the energy hub without consideration of the investment cost for operation and maintenance. We consider the electricity and gas price signals to guide users to participate in the demand side response and adjust the energy structure. The energy purchase cost is:

$$F_1 = \sum_{t=1}^T (C_t^e P_t^{grid} + C_t^g Q_t^{gas}) \quad (17)$$

where  $P_t^{grid}$  is the amount of power exchanged between the energy hub and the external grid at time  $t$ ;  $Q_t^{gas}$  is the amount of natural gas purchased at time  $t$ ;  $C_t^e$  is the external grid price;  $C_t^g$  is the natural gas price; and  $T$  is the time period for the economic dispatch cycle. To tackle the day-ahead dispatch problem, we take  $T$  as 24 hours.

We denote  $P_t^b$  as the electricity for buying (positive values) and  $P_t^s$  for selling (negative values), so we can obtain:

$$P_t^{grid} = P_t^b + P_t^s \quad (18)$$

The purchase-sale price ratio can be set to be  $C_t^{buy} : C_t^{sell} = 1.3$  in simulations [5]. In normal circumstances, this value should be set between 1 and 2 based on experience. In this paper, we set the ratio to be 1.3, which is actually a rough ratio for validation. Then, we can obtain:

$$Q_t^{gas} = \beta P_t^{gas} \quad (19)$$

where  $\beta$  is the conversion factor denoting the natural gas amount required for 1 kWh. Usually, we take  $\beta$  as 0.0925, which means we require 0.0925 m<sup>3</sup> to produce 1 kWh power [5].

##### 2) Environmental Cost

The energy hub consumes electricity and natural gas supplied from external sources. The objective function of minimizing the carbon emissions is:

$$\min F_2 = \sum_{t=1}^T [Q_t^{gas} (\mu_{CO_2}^{gas} C_{CO_2} + \mu_{NO_x}^{gas} C_{NO_x} + \mu_{SO_x}^{gas} C_{SO_x}) + P_t^{grid} (\mu_{CO_2}^{grid} C_{CO_2} + \mu_{NO_x}^{grid} C_{NO_x} + \mu_{SO_x}^{grid} C_{SO_x})] \quad (20)$$

where  $\mu$  is the unit emission coefficient, the unit is g/kWh for electricity, and g/m<sup>3</sup> for natural gas;  $Q_t^{gas}$  is the gas purchase volume of the energy hub at time  $t$ ; and  $C$  is the unit treatment cost of the pollutants. The total objective function is:

$$\min F = \omega_1 F_1 + \omega_2 F_2 \quad (21)$$

where  $\omega_1 = \omega_2 = 1$ , denoting the equal importance of two objectives.

#### B. Constraints

##### 1) Power Balance Constraints

As shown in Fig. 1, the electricity-heating-cooling power balance constraints can be given as:

$$\begin{cases} L_t^e + P_t^{EB} + P_{e,t}^{ch} + P_{com,t}^{ch} = P_t^{grid} + P_t^{WT} + P_t^{PV} + P_t^{MT} + P_{e,t}^{dis} + \eta_e^{com} P_{com,t}^{dis} \\ L_t^h + P_t^{AC} + P_{h,t}^{ch} = P_{h,t}^{CHP} + \tilde{P}_t^{EB} + \tilde{P}_t^{GB} + P_{h,t}^{dis} + \eta_h^{com} P_{com,t}^{dis} \\ L_t^c = \tilde{P}_t^{AC} + \eta_c^{com} P_{com,t}^{dis} \end{cases} \quad (22)$$

where  $L_t^e$ ,  $L_t^h$ , and  $L_t^c$  are the total electricity load, heating load, and cooling load at time  $t$ , respectively;  $P_{e,t}^{ch}$ ,  $P_{h,t}^{ch}$  and  $P_{com,t}^{ch}$  are the charging power of the ES, HS, and NSF-CAES, respectively;  $P_{e,t}^{dis}$ ,  $P_{h,t}^{dis}$  and  $P_{com,t}^{dis}$  are the discharging power of the ES, HS, and NSF-CAES, respectively;  $\eta_e^{com}$  and  $\eta_h^{com}$  are the efficiencies of converting NSF-CAES energy into electricity and heating, respectively; and  $P_t^{WT}$ ,  $P_t^{PV}$ ,  $P_t^{CHP}$ ,  $P_t^{grid}$ , and  $P_t^{gas}$  are the power outputs of the wind turbine, solar panel, CHP, electricity, and natural gas, respectively.

##### 2) CHP Power and Ramp Rate Constraints

For the CHP, the power and ramp rates meet the constraints:

$$\begin{cases} P_{min}^{CHP} \leq P_t^{CHP} \leq P_{max}^{CHP} \\ -\Delta P_{down}^{CHP} \leq P_t^{CHP} - P_{t-1}^{CHP} \leq \Delta P_{up}^{CHP} \end{cases} \quad (23)$$

where  $P_{max}^{CHP}$  and  $P_{min}^{CHP}$  are the upper and lower limits of the natural gas power consumption, respectively; and  $\Delta P_{up}^{CHP}$  and  $\Delta P_{down}^{CHP}$  are the maximum rates of ramping up and down, respectively.

##### 3) EB, GB, and AC Constraints

The input energies of EB, GB, and AC are different, but they meet the same power constraints as:

$$P_{min}^{EB,GB,AC} \leq P_t^{EB,GB,AC} \leq P_{max}^{EB,GB,AC} \quad (24)$$

where  $P_{min}^{EB,GB,AC}$  and  $P_{max}^{EB,GB,AC}$  are the lower and upper limits of EB, GB, and AC, respectively.

##### 4) ES/HS Equipment Constraints

In addition to the operating mode of (2), the energy storage equipment should meet the following constraints:

$$\begin{cases} E_{min} \leq E_t \leq E_{max} \\ 0 \leq P_t^{ch} \leq \delta_t^{ch} P_{max}^{ch} \\ 0 \leq P_t^{dis} \leq \delta_t^{dis} P_{max}^{dis} \\ \delta_t^{ch} + \delta_t^{dis} \leq 1 \\ E_1 \leq E_T \end{cases} \quad (25)$$

where  $E_{max}$  and  $E_{min}$  are the upper and lower limits of the stored energy, respectively;  $\delta_t^{ch}$  and  $\delta_t^{dis}$  are the normalized charging and discharging states, respectively;  $P_{max}^{ch}$  and  $P_{max}^{dis}$  are the maximum charging and discharging rates of each time interval, respectively;  $\delta_t^{ch} + \delta_t^{dis} \leq 1$  indicates that at any time, the storage equipment can only charge or discharge; and  $E_1 \leq E_T$  means that the energy reserve at the end of the cycle  $E_T$  should be equal or larger than the initial energy  $E_1$ .

##### 5) NSF-CAES Constraints

If NSF-CAES adopts an STW-based system-level modeling method, we need to make further constraints in this modeling method. This enables the NSF-CAES to participate in the dispatch process of the micro-energy grid in a reasonable manner.

Considering the large inertia of NSF-CAES, its dispatch strategy is designed as:

$$\begin{cases} E_{com}^{ch} = P_{com,t}^{ch} \Delta T_{ch} \\ E_{com}^{dis} = P_{com,t}^{dis} \Delta T_{dis} \\ \Delta T_{ch} \geq A \\ \Delta T_{dis} \geq B \\ \Delta T_{ch} \succ \Delta T_{dis} \end{cases} \quad (26)$$

where  $E_{com}^{ch}$  and  $E_{com}^{dis}$  are the total charging and discharging energies of NSF-CAES, respectively;  $\Delta T_{ch}$  and  $\Delta T_{dis}$  are the energy charging and discharging periods, respectively;  $A$  and  $B$  are the minimum time periods required for energy storage and release, respectively; and  $\Delta T_{ch} \succ \Delta T_{dis}$  denotes that the energy should be charged first and then discharged. We assume that NSF-CAES has no energy storage at the beginning and is charging in higher-price period while discharging in lower-price period.

### C. Optimization Problem Formulation

If the NSF-CAES adopts component-level modeling, it will directly join the dispatch process and participate in dispatch together with other equipment. If the NSF-CAES adopts STW-based system-level modeling, it will be dispatched separately from other equipment. We focus on the superiority of STW-based NSF-CAES system-level modeling for dispatch. The analysis of the dispatch results obtained by the two NSF-CAES modeling methods will be given in Section V. According to (1)-(26), the optimization problem for the micro-energy grid can be described as:

$$\begin{cases} \min(F_1(\mathbf{x}), F_2(\mathbf{x})) \\ \text{s.t. } \mathbf{h}(\mathbf{x}) = \mathbf{0} \\ \mathbf{g}(\mathbf{x}) \leq \mathbf{0} \end{cases} \quad (27)$$

where  $F_1(\mathbf{x})$  is the total economic cost;  $F_2(\mathbf{x})$  is the environmental cost;  $\mathbf{h}(\mathbf{x})$  and  $\mathbf{g}(\mathbf{x})$  are the equality and inequality constraints, respectively; and  $\mathbf{x}$  is the vector of the decision variables for all time periods. Actually, this is a non-linear programming problem and is difficult to solve using off-the-shelf solvers like CPLEX and Gurobi. Therefore, an intelligent algorithm named DE-HSS is adopted.

## IV. DISPATCH USING STW AND DE-HSS

### A. Operation Time Determination of NSF-CAES Using STW

The NSF-CAES uses compressed air for heating supply and low-temperature gas for cooling. It enables clean and efficient electrical energy storage without fuel after burning [10]. Compared with CAES, it coordinates cooling, heating, and electricity flexibly. But it cannot start or stop frequently, and frequent charging or discharging will aggravate its degradation. So the operation time should be properly dispatched. Some methods compute the operation time during the optimization using heuristic algorithms or linear programming. In comparison, we use the STW to determine the working period of NSF-CAES before dispatch. This method is suitable for system-level modeling of NSF-CAES and is shown in Fig. 4.

In Fig. 4, the actual time of use (TOU) electricity and natural gas prices for 24 hours are listed in layer 1. For example, we take the charging and discharging time window as 2

hours, and charge or discharge the NSF-CAES twice a day because of the two power peaks at noon and night. Similarly, by sliding layer 2 to layer 23, the dispatch of NSF-CAES is realized. Obviously, if the time window length is 2 hour, we can get 23 windows by using the STW method. Inside each window, we compute the sum of TOU electricity and natural gas prices. For example, the sum value of the 1<sup>st</sup> window is  $E_1 + E_2 + G_1 + G_2$ . Thus we can get totally 23 values, which constitute a constant scalar called comprehensive energy price (CEP).

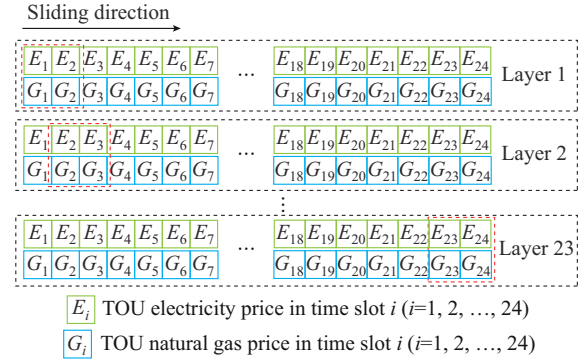


Fig. 4. Schematic diagram for STW.

To determine the CEP, we first denote  $T_i$  as the time window  $i$ , where  $length(T_i)=2$ . Then, we slide the window. As shown in Fig. 4, sliding layer 1 to layer 2 is called one-step sliding. Continue slide until the end condition is satisfied, i.e., to the end time slot 24. After each step, compute the current window CEP as  $sum(T_i)$ :

$$\begin{cases} sum(T_i) = T\_EP(T_i) + T\_GP(T_i) \\ T\_EP(T_i) = T\_EP(t_i) + T\_EP(t_{i+1}) \\ T\_GP(T_i) = T\_GP(t_i) + T\_GP(t_{i+1}) \\ T_i = 1, 2, \dots, 23 \\ t_i = 1, 2, \dots, 24 \end{cases} \quad (28)$$

where  $T\_EP$  is TOU electricity price;  $T\_GP$  is TOU natural gas price; and  $t_i$  is the dispatch time length.

To make the NSF-CAES charge in the minimum period and discharge in the maximum period, we set four windows:

$$\begin{cases} \min 1: T_1 \leq T_{\min 1} \leq T_{17} \\ \max 1: T_{\min 1} \leq T_{\max 1} \leq T_{19} \\ \min 2: T_{\max 1} \leq T_{\min 2} \leq T_{21} \\ \max 2: T_{\min 2} \leq T_{\max 2} \leq T_{23} \end{cases} \quad (29)$$

where min1 and max1 make the first couple of charging/discharging windows; and min2 and max2 make the second couple of windows, e.g.,  $T_{\min 1}$  is the minimum period of first charging window. For the first inequality, when the charging time is selected, there must be at least 6 hours left for the other three windows. So the window number is no more than 17. For the second inequality, there must be at least 4 hours left for the other two windows. So the window number is no more than 19. For the third inequality, the window number is no more than 21. For the last inequality, 23 is the threshold of the loop. Obviously, STW is a straightforward

and effective way without frequently starting and stopping equipment during the dispatch process. This helps extend the service life of NSF-CAES.

Experiments show that decreasing the window size, e.g., from 4 to 2, or increasing the window size, e.g., from 4 to 6, is not preferable. Smaller window size will lead to the increase of overall energy cost due to the absence of energy provided by the NSF-CAES during load peaks while the TOU electricity or natural gas price is relatively higher. Larger window size can reduce the energy cost to a very limited degree but frequent charging and discharging of NSF-CAES will deteriorate the life of NSF-CAES. Thus we adopt the four-window scheme in case studies.

### B. Optimization Using DE-HSS Algorithm

The HSS has been proven effective in optimizing complex linear or non-linear systems [29]. However, it sometimes tends to the local optimum. The seeking process of the HSS particles lacks intelligent mechanism, leading to more time cost but less accurate computation. Thus, we improve the HSS algorithm with the DE, called DE-HSS. The basic steps for the DE-HSS are as follows.

#### 1) Step 1: Particle Initialization

1) Define the initial population number  $N_{pop}$ , the number of hyper-sphere centers (SCs)  $N_{SC}$ , the upper and lower limits of the HSS radius  $r_{max}$  and  $r_{min}$ , and angle change probability  $Pr_{angle}$ .

2) A set of initial solutions is randomly generated. The decision variable  $x_i$  is randomly selected from  $[X_{i,min}, X_{i,max}]$  with a uniform probability. The solutions are called particles, whose objective functions are calculated accordingly.

3) The particles are represented by  $\mathbf{P}=[p_1, p_2, \dots, p_N]$ , where  $p_i$  ( $i=1, 2, \dots, N$ ) is the decision variable. The objective functions for the particles are determined as  $f(\mathbf{P})$ . The particles are sorted in the ascending order based on their objective function values. The best  $N_{SC}$  particles (at the top of the list) are selected as SCs.

4) The remaining particles are dominated by SCs. To divide the particles proportionally, the objective function difference (OFD) of each SC is defined as the difference between the value of the SC objective function and the maximum objective function value of SCs. That is,  $OFD_{SC} = f_{SC} - \max_{SC} \{f\}$ , where  $\max_{SC} \{f\}$  is the SC with the largest value among all the objective function values corresponding to SCs. Thus, the normalized dominance of each SC is defined as:

$$D_{SC} = \left| \frac{OFD_{SC}}{\sum_{i=1}^{N_{SC}} OFD_i} \right| \quad (30)$$

where  $OFD_{SC}$  is the OFD of a certain SC; and  $OFD_i$  is the OFD of SC  $i$ .

Then, the initial number of particles, which belongs to an SC, will be equal to  $round\{D_{SC}(N_{pop} - N_{SC})\}$ , and will be chosen randomly by each SC from the remaining particles.

#### 2) Step 2: Searching

1) A particle seeks a better solution within the bounded sphere with the predefined center. The sphere radius  $r$  de-

notes the distance between the particle and the center. The origin is set at the sphere center. The searching program is performed with varying particle parameters (the radius  $r$  and angle  $\theta$ ).

2) There are  $N-1$  angles for the  $N$ -dimension problem. Any varying angle will cause the particle movement in the searching space. For the DE-HSS, each angle  $\theta$  changes by  $\alpha$  radians, and the probability of each radian change is  $Pr_{angle}$ .  $\alpha$  is randomly selected between  $(0, 2\pi)$  with uniform distribution.

3) After changing all angles of the particle, the distance between the particle and the center is randomly chosen in  $[r_{min}, r_{max}]$ . In the  $N$ -dimension hyper-sphere,  $r$  is calculated as:

$$r^2 = \sum_{i=1}^N (p_{i,center} - p_{i,particle})^2 \quad (31)$$

where  $p_{i,center}$  is the center of a hyper-sphere in  $i$ -dimension; and  $p_{i,particle}$  is the particle belongs to a certain center in  $i$ -dimension.

After changing  $\theta$  and  $r$ , together with evaluating  $f$ , the searching process of particles in the space is completed.

4) If there exists a particle whose position becomes lower than the SC, we then use it to take the place of the SC.

#### 3) Step 3: DE

Compared with HSS, the DE-HSS uses this step to enhance the searching ability while ensuring the computation accuracy.

1) For each particle belonging to an SC, if  $rand > MR$  ( $MR$  is the mutation rate), we can obtain:

$$P = q_1 + F(q_3 - q_2) + rand \cdot (SC_{best} - q) \quad (32)$$

where  $q_1$ ,  $q_2$ , and  $q_3$  are three randomly selected particles;  $F$  is the scaling factor;  $SC_{best}$  is the best hyper-spherical center, i.e., the globally optimal center;  $rand$  is a random value between 0 and 1; and  $q$  is the mutation particle.

2) If  $CR > rand$  ( $CR$  is the crossover rate), judge whether to perform differential crossover by using:

$$D_i = \begin{cases} P_i & rand < CR \\ q_i & otherwise \end{cases} \quad (33)$$

3) Calculate the objective function of the new particle, and update the particle if the value is smaller than the original particle.

4) Compare the objective function of all the changed particles to reselect SC.

#### 4) Step 4: Dummy Particles Recovery

The particles searched within inappropriate spaces are called dummy particles.

1) Particle sets should be classified according to their set objective function (SOF) to seek the worst set with dummy particles. The SOF of a set is mainly affected by the objective function of SC  $f_{SC}$ , and the objective function of the particles is less important. Thus, we define the SOF for each group as:

$$SOF = f_{SC} + \gamma \cdot mean\{f_{particles, SC}\} \quad (34)$$

where  $mean\{f_{particles, SC}\}$  is the mean value of the objective function values of all particles dominated by a certain SC.

A small  $\gamma$  ensures that a set of SOFs can be determined by the objective function of SC. Increasing  $\gamma$  will increase

the role of the particles in determining the SOF.

2) The process of dummy particles recovery is modeled by selecting some dummy particles from the hyper-spheres with the largest SOF and assigning them to other SCs. The difference in the SOF (DSOF) of each group is expressed by:

$$DSOF = SOF - \max \{SOF\} \quad (35)$$

where  $\max \{SOF\}$  is the maximum value among all SOFs. Then, particles can be assigned to one of the SCs with the calculated DSOF.

3) Calculate the assigning probability (AP) for each SC:

$$AP = \left| \frac{NTOF}{\sum_{i=1}^{N_{SC}} NTOF_i} \right| \quad (36)$$

where  $NTOF$  is the normalized total objective function. The set  $AP = \{AP_1, AP_2, \dots, AP_{N_{SC}}\}$  divides the particles in SCs based on their APs. The dummy particles are assigned to the SC  $i$  with a probability of  $AP_i$ . Thus, the worst group (with the highest SOF) will lose its dummy particles. The particles seek a new SC in all SCs based on their AP. If an SC has no particles, it will be treated as a particle and a new SC will be set.

5) *Step 5: Redefine SCs*

At the end of each iteration, all particles and SCs are sorted according to their objective function values. The best particles are selected as the new SCs for the next iteration.

6) *Step 6: Judge and Output*

The loop will be terminated in the case of one of the conditions as follows.

- 1) Reach the maximum number of iteration.
- 2) The iteration error is lower than the preset threshold, e.g.,  $10^{-5}$ . The optimal value is then obtained as the final output.

The deficit of the traditional HSS can be observed in *Step 2*, where  $\alpha$  is randomly selected for one iteration. Moving the particles according to this rule may lead to the local optima. *Step 3* formulates the hybrid DE-HSS using the differential mutation of DE, so particles are distributed with increased diversity. Meanwhile, the differential crossover is performed to retain the differentially mutated particles to avoid unnecessary computation. Although the DE-HSS may take a longer period for one iteration, the total iteration number required to seek the optimal solution is reduced. In addition, after adding the DE step, the algorithm can effectively avoid falling into the local optima, so the searching ability is enhanced.

## V. CASE STUDIES AND COMPARATIVE ANALYSIS

### A. Case Studies

We make case studies on the proposed optimization scheme. The parameters of the computer are: Intel (R) Core (TM) i7-7500 CPU @ 2.70 GHz and 2.90 GHz, 4 GB RAM, 64 bit operating system, and MATLAB R2016a. The simulation interval is set as 1 hour.

Based on some existing studies [2], [5], [13], [20], the sys-

tem parameters are set using the data of community-level load and energy price. The wind and solar data come from the U.S. DOE [30]. Table I lists the parameters used for the simulation.

TABLE I  
PARAMETERS OF SYSSEM MODEL

Model	Parameters	Value
CHP	$P_{\max}^{CHP}, P_{\min}^{CHP}$	3000 kW, 0 kW
	$P_{\max}^{CHP}, P_{\min}^{CHP}$	1200 kW, 1200 kW
ES	$\eta_e^{ch}, \eta_e^{dis}, \eta_e^{loss}$	0.94, 0.94, 0.005
	$E_{\max}^e, E_{\min}^e$	600 kW, 0 kW
HS	$P_{\max}^{e, ch}, P_{\max}^{e, dis}$	150 kW, 150 kW
	$\eta_h^{ch}, \eta_h^{dis}, \eta_h^{loss}$	0.96, 0.96, 0.01
EB	$E_{\max}^h, E_{\min}^h$	500 kW, 0 kW
	$P_{\max}^{h, ch}, P_{\max}^{h, dis}$	125 kW, 125 kW
EB	$\eta_h^{EB}, P_{\max}^{EB}, P_{\min}^{EB}$	0.85, 1000 kW, 0 kW
GB	$\eta_h^{GB}, P_{\max}^{GB}, P_{\min}^{GB}$	0.8, 3500 kW, 0 kW
AC	$\eta_c^{AC}, P_{\max}^{AC}, P_{\min}^{AC}$	0.98, 1500 kW, 0 kW
NSF-CAES	$\eta_{com}^{ch}, \eta_{com}^{dis}, \eta_{com}^{loss}$	0.95, 0.95, 0.05
	$\eta_c^{com}, \eta_h^{com}, \eta_e^{com}$	0.47, 0.24, 0.245
Pollution coefficient	$A, B$	2 hours, 2 hours
	$\mu_{CO_2}^{grid}, \mu_{NO_x}^{grid}, \mu_{SO_x}^{grid}$	968 g/kWh, 2.5 g/kWh, 0.1 g/kWh
Pollution coefficient	$\mu_{CO_2}^{gas}, \mu_{NO_x}^{gas}, \mu_{SO_x}^{gas}$	220 g/m <sup>3</sup> , 0.019 g/m <sup>3</sup> , 0.000262 g/m <sup>3</sup>
	$C_{CO_2}, C_{NO_2}, C_{SO_2}$	0.025 CNY/kg, 8 CNY/kg, 6 CNY/kg

The power unit is uniformly converted to kW. For calculation convenience, the initial SOCs for ES and HS are both set to be 50%. The minimum reserve is 10%. The maximum charging or discharging energy of NSF-CAES per hour is set to be 500 kW after unit commitment analysis. The price unit is CNY. The power outputs of wind and solar energy are shown in Fig. 5.

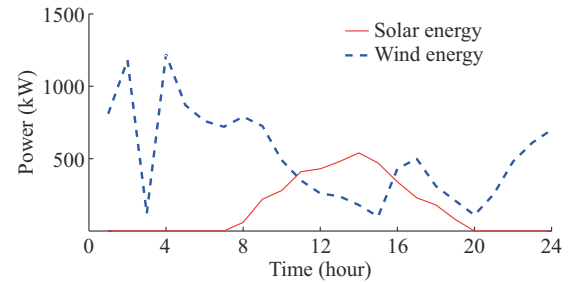


Fig. 5. Power outputs of wind and solar energy.

Figure 6 shows the information of electricity load, cooling load, and heating load [31]. The peak loads appear in the evening, night, and noon, respectively.

Figure 7 shows the TOU electricity price and natural gas price. The price of the electricity or natural gas energy is set based on the Australian Energy Market Operator (AEMO) in Victoria on a certain day [32]. It can be observed that the energy prices are generally higher during periods of high energy usage. This encourages users to participate in demand response and makes efficient use of hybrid energies.

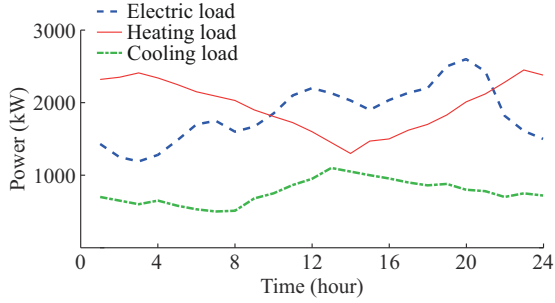


Fig. 6. Information of electric load, cooling load, and heating load.

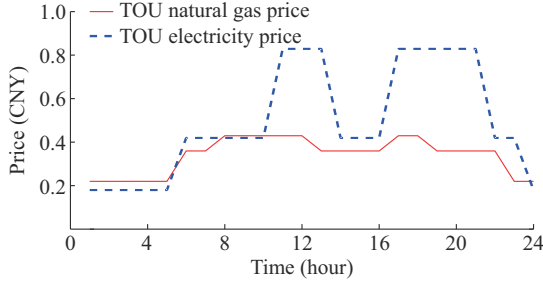


Fig. 7. TOU electricity and natural gas prices.

We first analyze the performance of different modeling methods of NSF-CAES in the calculation examples. Without consideration of the energy storage at the beginning, we list the parameters required for NSF-CAES “STW-based system-level modeling” and “component-level modeling”, as given in Tables I and II, respectively. Other relevant parameter settings can be found in [10].

TABLE II  
PARAMETERS OF NSF-CAES COMPONENT-LEVEL MODELING

Parameter	Value
Compressor rated power	500 kW
$T_1$	190 °C
$Q_{m,c}$	0.77 kg/s
Turbine rated power	500 kW
$Q_{m,e}$	1.54 kg/s

We analyze the two modeling methods by considering the two-objective function as an example. With the proposed DE-HSS, the parameters of the methods have been optimized. The optimization results are shown in Table III.

TABLE III  
RESULT COMPARISON OF DIFFERENT NSF-CAES MODELING METHODS

Method	Modeling method	Cycle times	Optimal time to threshold (s)	Cost (CNY)
I	Component-level	4 (calculated)	48.7	39185.1
II (proposed)	STW-based system-level	2 (predefined)	40.2	39220.5

First, it can be observed from Table III that for the optimal solution using method I, the NSF-CAES runs for 4 cycles. In comparison, the optimal solution using method II

runs for 2 cycles, which helps avoid unnecessary charging or discharging and prolong the storage life to some extent. Second, for method I, the NSF-CAES and other devices are dispatched together, so the calculation time to find the optimal solution is longer than method II. Finally, although the optimal solution using method I reduces a certain cost, the frequent dispatch of NSF-CAES will have negative effect on its lifespan. Using method II is simpler and easier to adjust, without fluctuations in the dispatch process in case of failure. So method II has potentiality for engineering applications.

For method I, we use the genetic algorithm to perform simulation analysis. The results show that the NSF-CAES still dispatches 4 cycles, but the genetic algorithm (GA) leads to larger computation time. The optimal time to threshold and total cost compared with the proposed DE-HSS algorithm are shown in Table IV.

TABLE IV  
COMPARISON BETWEEN GA AND DE-HSS

Algorithm	Optimal time to threshold (s)	Cost (CNY)
GA	52.1	39200.6
DE-HSS	48.7	39185.1

Further, we make comparative simulations with different scenarios using method II for detailed validation. Three scenarios are used as follows.

- 1) Scenario 1: economic and environmental cost optimization.
- 2) Scenario 2: economic cost optimization.
- 3) Scenario 3: environmental cost optimization.

Based on the proposed model and scheme, the power dispatch results of the nine components are shown as follows.

Figure 8 shows the one-day dispatch results for scenario 1.

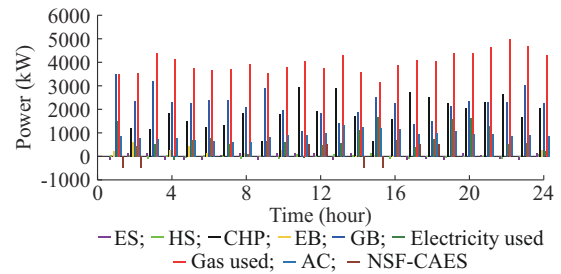


Fig. 8. One-day dispatch results for scenario 1.

Due to the renewable energy supplement and less power consumption, the ES will be charged during night at 15:00-17:00 with negative values. At 10:00-12:00 and 20:00-21:00, it is discharged with positive values. At 04:00, the electricity usage is negative, denoting selling electricity to electricity company. During 14:00-15:00 and 19:00-21:00, the electricity usage increases, and this fits the two electricity load peaks in Fig. 6. In other periods, ES operates to reduce peak and fills valley based on the TOU electricity price. During the night and morning, the GB provides more power output.

During the two peaks of electricity consumption, the CHP output decreases due to its lower efficiency.

As indicated in Fig. 6, the heating load is high during 01:00-03:00 and 22:00-24:00 because of increased heating consumption, so the HS releases the heating correspondingly. The cooling load affects the AC output, and the CEP determines the charging and discharging of the NSF-CAES. It can be observed in Fig. 8 that the NSF-CAES charges or discharges exactly at the peak or valley of the CEP, and this enables the energy consumption optimization.

For scenarios 2 and 3, the trends of electricity and natural gas usage are basically the same as scenario 1. But for scenario 2 shown in Fig. 9, only the economic cost is considered, so the power output time of the EB becomes longer when the total output increases significantly. The overall electricity usage is higher while the total natural gas usage is lower than scenario 1. For scenario 3 shown in Fig. 10, only the environmental cost is minimized, so the CHP ramps up rapidly to the value where the maximum energy can be supplied. The EB output is correspondingly less, and the system consumes more gas but less electricity than scenario 1. This also leads to an increase of electricity sales.

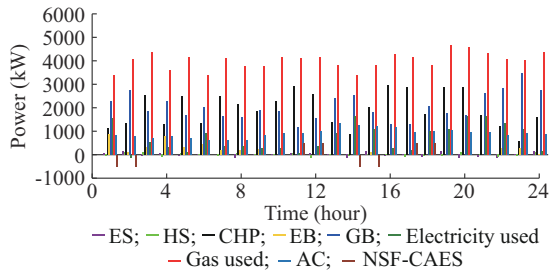


Fig. 9. One-day dispatch results for scenario 2.

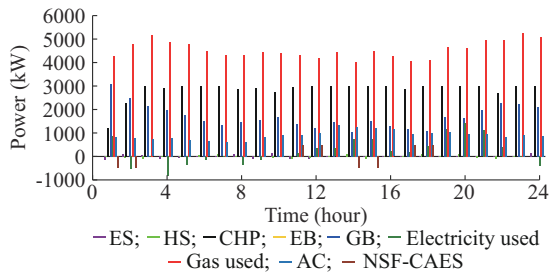


Fig. 10. One-day dispatch results for scenario 3.

Table V compares the energy consumption for the three scenarios by taking the average values of multiple experiments. According to (17), (20), and (21), we have the economic cost  $F_1$ , environmental cost  $F_2$ , and the total cost  $F_{tot}$  (i.e.,  $F_1+F_2$ ). Obviously, the total cost  $F_{tot}$  of scenario 1 is less than those of scenarios 2 and 3 which only considers the economic cost or environmental cost separately. For the electricity usage, which is relatively cheaper but may lead to more pollution, scenario 2 has the bigger value whereas scenario 3 has the smallest value because of minimizing the environmental cost. Similarly, for the natural gas usage which is environmentally friendly but more expensive, scenario 2 has the smallest value and scenario 3 has the most. Thus,

multi-objective optimization (scenario 1) achieves the smallest overall cost with balanced electricity and natural gas usage.

TABLE V  
COMPARISONS OF ENERGY CONSUMPTION FOR THREE SCENARIOS

Scenario	Cost (CNY)	Electricity usage (kW)	Natural gas usage (kW)	Electricity and natural gas usage (kW)
1	39221	14112	99291	113403
2	38889+763	16999	96323	113322
3	41434+151	5339	109585	114924

### B. Comparative Studies

We compare the DE-HSS with weighted particle swarm algorithm (WPSO), ICA, and HSS using scenario 1. The parameters have been tuned optimally, as listed in Table VI.

TABLE VI  
ALGORITHM PARAMETERS

Algorithm	Parameter	Value
WPSO	$N_{pop}$ , $w$ , $w_{damp}$ , $c_1$ , $c_2$	500, 1, 0.99, 2, 2
ICA	$N_{pop}$ , $N_{emp}$ , $\alpha$ , $\beta$ , $P_{rev}$ , $\mu$ , $\zeta$	100, 10, 1, 1.5, 0.05, 0.1, 0.2
HSS	$N_{particle}$ , $N_{SC}$ , $r_{contdown}$ , $r_{contup}$ , $\zeta$ , $Num$	1000, 50, 0, 1.1, 0.05, 5
DE-HSS	$N_{particle}$ , $N_{SC}$ , $r_{contdown}$ , $r_{contup}$ , $\zeta$ , $Num$ , $F$ , $MR$ , $CR$	1000, 50, 0, 1.1, 0.05, 5, 0.5, 0.3, 0.9

For WPSO,  $w$  is the inertia weight;  $w_{damp}$  is the variable weight coefficient; and  $c_1$  and  $c_2$  are the learning factors. For ICA,  $N_{emp}$  is the number of imperialist countries;  $P_{rev}$  is the revolution probability;  $\mu$  is the revolution rate; and  $\zeta$  is colony mean cost coefficient. For HSS,  $N_{particle}$  and  $N_{SC}$  are the total particle number and SC number, respectively;  $r_{contdown}$ ,  $r_{contup}$  and  $r_{contup}$  are the lower limit and upper limits of the hyper-sphere radius, respectively;  $\zeta$  is the dummy particle parameter; and  $Num$  is the dummy particle number for each iteration. For DE-HSS, we use  $F$  to denote the scaling factor.  $MR$  and  $CR$  denote the mutation probability and crossover probability, respectively. The results for 500 times of iterations are shown in Figs. 11 and 12.

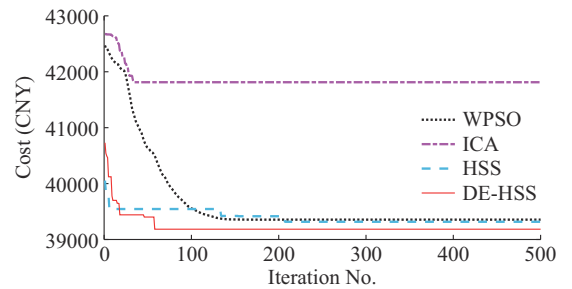


Fig. 11. Convergence of four algorithms.

It can be observed that the DE-HSS shows the best convergence performance in Fig. 11. Figure 12 indicates that the particle mean value of DE-HSS is the least, so it obtains the

optimal solution easily. We perform multiple tests with the iteration threshold as 0.001 and list the average values in Table VII.

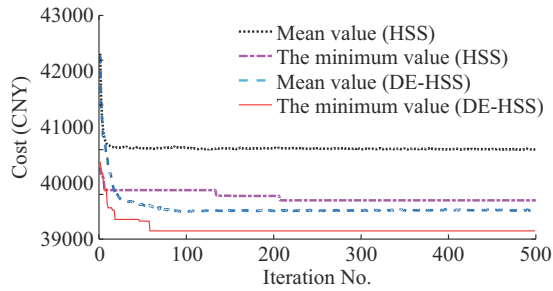


Fig. 12. Comparison for DE-HSS and HSS.

TABLE VII  
SEARCHING ABILITY AND SPEED OF ALGORITHMS

Algorithm	Optimal solution (CNY)	Optimal time to threshold (s)
WPSO	39353.2	39.4
ICA	42601.8	15.1
HSS	39316.9	80.6
DE-HSS	39220.5	40.2

It is observed that both the searching ability and searching speed of the DE-HSS are better than the HSS. The ICA converges the fastest but shows the worst accuracy. The WPSO converges faster than HSS and DE-HSS but slower than ICA. The DE-HSS has the best searching ability, but takes a longer convergence time. Note that the time consumption is acceptable for the hour-level dispatch scenarios, and can be potentially applied in day-ahead optimization applications.

In addition, the selection of parameters in the DE step of DE-HSS will also affect the performance of the algorithm. Through multiple experiments, we get the following conclusions.

1) Keep  $MR$  and  $CR$  fixed, and change  $F$ : a smaller  $F$  enables faster convergence, but when  $F$  deviates from the optimal value, the seeking accuracy will decrease.

2) Keep  $MR$  and  $F$  fixed, and change  $CR$ : a larger  $CR$  enables faster convergence, but when  $CR$  deviates from the optimal value, the seeking accuracy will decrease.

3) Keep  $CR$  and  $F$  fixed, and change  $MR$ : a larger  $MR$  enables faster convergence, but when  $MR$  deviates from the optimal value, the seeking accuracy will decrease.

## VI. CONCLUSION

We focus on two key issues in existing energy hub based micro-energy grid: utilizing new storage equipment and improving the optimization algorithm. The key conclusions are summarized as follows.

Firstly, at the model level, we introduce the NSF-CAES into the energy hub and perform an accurate component-level modeling. Furthermore, to prolong the life of NSF-CAES and make it easy to adjust, we propose a system-level modeling of NSF-CAES and use the STW method for dispatch. Comparative numerical examples are performed to show the

superiority of the designed STW method. Then, at the algorithm level, considering the complex model and non-linear optimization problem, the improved HSS algorithm named DE-HSS is used for optimization. The DE-HSS has well balanced convergence speed and optimization accuracy, with enhanced global searching ability and higher probability of the proper searching direction. Finally, we perform three simulation scenarios for multi-objective analysis on the micro-energy grid, demonstrating the superiorities of the proposed STW and DE-HSS optimization algorithm. Future studies may focus on multiple micro-energy grid dispatch to solve the problem of energy coordination in multiple regions.

## REFERENCES

- [1] T. Ma, J. Wu, and L. Hao, "Energy flow modeling and optimal operation analysis of the micro energy grid based on energy hub," *Energy Conversion and Management*, vol. 133, no. 1, pp. 292-306, Feb. 2017.
- [2] M. Geidl and G. Andersson, "Optimal power flow of multiple energy carriers," *IEEE Transactions on Power Systems*, vol. 22, no. 1, pp. 145-155, Feb. 2007.
- [3] F. T. Muhammad, H. Chen, M. Kashif *et al.*, "Integrated energy system modelling of China for 2020 by incorporating demand response, heat pump and thermal storage," *IEEE Access*, vol. 7, pp. 40095-40108, Mar. 2019.
- [4] S. Beigvand and H. Abdi, "A general model for energy hub economic dispatch," *Applied Energy*, vol. 190, no. 1, pp. 1090-1111, Jun. 2017.
- [5] F. Brahman and M. Honarmand, "Optimal electrical and thermal energy management of a residential energy hub integrating demand response and energy storage system," *Energy and Buildings*, vol. 90, no. 1, pp. 65-75, Mar. 2015.
- [6] D. Setlhaolo, S. Sichelalu, and J. Zhang, "Residential load management in an energy hub with heat pump water heater," *Applied Energy*, vol. 13, no. 2, pp. 100-108, Oct. 2017.
- [7] M. J. Sanjari, H. Karami, A. H. Yatim *et al.*, "Application of hyper-spherical search algorithm for optimal energy resources dispatch in residential microgrids," *Applied Soft Computing*, vol. 3, no. 1, pp. 1-8, Jul. 2015.
- [8] S. Moazeni, A. H. Miragha, and B. Defourny, "A risk-averse stochastic dynamic programming approach to energy hub optimal dispatch," *IEEE Transactions on Power Systems*, vol. 34, no. 3, pp. 2169-2178, May 2019.
- [9] Y. Li, H. Zhang, X. Liang *et al.*, "Event-triggered-based distributed cooperative energy management for multi energy systems," *IEEE Transactions on Industrial Informatics*, vol. 15, no. 4, pp. 2008-2022, Apr. 2019.
- [10] R. Li, L. Chen, T. Yuan *et al.*, "Optimal dispatch of zero-carbon-emission micro Energy Internet integrated with non-supplementary fired compressed air energy storage system," *Journal of Modern Power Systems and Clean Energy*, vol. 4, no. 4, pp. 566-580, Oct. 2016.
- [11] Y. Li, J. Wang, Y. Han *et al.*, "Robust and opportunistic scheduling of district integrated natural gas and power system with high wind power penetration considering demand flexibility and compressed air energy storage," *Journal of Cleaner Production*, vol. 256, no. 1, pp. 1-19, May 2020.
- [12] Y. Li, S. Miao, X. Luo *et al.*, "Dynamic modelling and techno-economic analysis of adiabatic compressed air energy storage for emergency back-up power in supporting microgrid," *Applied Energy*, vol. 261, no. 1, pp. 1-16, Mar. 2020.
- [13] J. Bai, L. Chen, F. Liu *et al.*, "Interdependence of electricity and heat distribution systems coupled by an AA-CAES-based energy hub," *IET Renewable Power Generation*, vol. 14, no. 3, pp. 399-407, Mar. 2020.
- [14] H. Fontenot and B. Dong, "Modeling and control of building-integrated microgrids for optimal energy management—a review," *Applied Energy*, vol. 254, no. 1, pp. 1-21, Nov. 2019.
- [15] M. F. Zia, E. Elbouchikhi, and M. Benbouzid, "Microgrids energy management systems: a critical review on methods, solutions, and prospects," *Applied Energy*, vol. 222, no. 15, pp. 1033-1055, Jul. 2018.
- [16] M. S. Misaghian, M. Saffari, M. Kia *et al.*, "Tri-level optimization of industrial microgrids considering renewable energy sources, combined heat and power units, thermal and electrical storage systems," *Energy*, vol. 161, no. 1, pp. 396-411, Oct. 2018.

- [17] A. M. Jadhav and N. R. Patne, "Priority-based energy scheduling in a smart distributed network with multiple microgrids," *IEEE Transactions on Industrial Informatics*, vol. 13, no. 6, pp. 3134-3143, Dec. 2017.
- [18] C. Ju, P. Wang, L. Goel *et al.*, "A two-layer energy management system for microgrids with hybrid energy storage considering degradation costs," *IEEE Transactions on Smart Grid*, vol. 6, no. 6, pp. 6633-6645, Jun. 2017.
- [19] A. Papavasiliou, Y. Mou, L. Cambier *et al.*, "Application of stochastic dual dynamic programming to the real-time dispatch of storage under renewable supply uncertainty," *IEEE Transactions on Sustainable Energy*, vol. 9, no. 2, pp. 547-558, Apr. 2017.
- [20] A. Rabiee, M. Saeghi, and J. Aghaei, "Modified imperialist competitive algorithm for environmental constrained energy management of microgrids," *Journal of Cleaner Production*, vol. 202, no. 1, pp. 273-292, Nov. 2018.
- [21] P. Li, R. Li, and Y. Cao, "Multiobjective sizing optimization for island microgrids using a triangular aggregation model and the Levy-harmony algorithm," *IEEE Transactions on Industrial Informatics*, vol. 14, no. 8, pp. 3495-3505, Aug. 2018.
- [22] A. Heidari and S. Mirjalili, "Harris hawks optimization: algorithm and applications," *Future Generation Computer Systems*, vol. 1, no. 3, pp. 1-8, Jun. 2019.
- [23] Y. Jing, H. Wang, T. Chugh *et al.*, "Data-driven evolutionary optimization: an overview and case studies," *IEEE Transactions on Evolutionary Computation*, vol. 23, no. 3, pp. 442-458, Sept. 2018.
- [24] P. Li, R. Dargaville, Y. Cao *et al.*, "Storage aided system property enhancing and hybrid robust smoothing for large-scale PV systems," *IEEE Transactions on Smart Grid*, vol. 8, no. 6, pp. 2871-2879, Nov. 2017.
- [25] A. Yousef, L. Mahmoud, and S. Yousef, "GICA: imperialist competitive algorithm with globalization mechanism for optimization problems," *Turkish Journal of Electrical Engineering and Computer Sciences*, vol. 25, no. 1, pp. 209-221, Nov. 2017.
- [26] N. Blair, A. P. Dobos, J. Freeman *et al.* (2020, Jun.). System advisor model, general description. [Online]. Available: [https://www.researchgate.net/publication/332031645\\_System\\_Advisor\\_Model\\_SAM\\_General\\_Description\\_Version\\_201795](https://www.researchgate.net/publication/332031645_System_Advisor_Model_SAM_General_Description_Version_201795)
- [27] D. Wu and R. Wang, "Combined cooling, heating and power: a review," *Progress in Energy and Combustion Science*, vol. 32, no. 5, pp. 459-495, Sept. 2006.
- [28] D. Zhang and T. Liu, "A multi-step modeling and optimal operation calculation method for large-scale energy hub model considering two types demand responses," *IEEE Transactions on Smart Grid*, vol. 10, no. 6, pp. 6735-6746, Apr. 2019.
- [29] H. Karami, M. J. Sanjari, and G. B. Gharehpetian, "Hyper-spherical search (HSS) algorithm: a novel meta-heuristic algorithm to optimize nonlinear functions," *Neural Computation & Applications*, vol. 26, no. 6, pp. 1455-1465, Nov. 2014.
- [30] U.S. Department of Energy. (2019, Jun.). Solar power data for integration studies. [Online]. Available: <https://energy.gov/eere/>
- [31] W. Zhang, C. Yang, K. Xie *et al.*, "ADMM-based distributed auction mechanism for energy hub scheduling in smart buildings," *IEEE Access*, vol. 6, pp. 45635-45645, Aug. 2018.
- [32] Australia Energy Market Operator (AEMO). (2020, May). Aggregated price and demand data. [Online]. Available: <http://www.aemo.com.au>

**Zhenlong Li** received the B.E. degree in automation from Hebei University, Baoding, China, in 2017. He is currently pursuing the Ph.D. degree in control science and engineering in Beijing Jiaotong University, Beijing, China. His research interests include modeling and scheduling analysis of integrated energy systems, multi-microgrid dispatch and design of power system forecasting method.

**Peng Li** received the Ph.D. degree from Harbin Institute of Technology, Harbin, China, in 2009. He undertook postdoctoral research at Beijing Jiaotong University, Beijing, China, from 2009 to 2011, and visiting research at University of Melbourne, Melbourne, Australia, from 2013 to 2014. He is with School of Electronic and Information Engineering, Beijing Jiaotong University. His research interests include automatic control, renewable energies, and smart grids.

**Jing Xia** received the M.S. degree from Harbin Institute of Technology, Harbin, China, in 2008. She worked at Goldwind Windenergy GmbH, Neunkirchen, Germany, from 2010 to 2011. She is currently pursuing the Ph.D. degree in North China Electric Power University, Beijing, China. She is also with Goldwind Science & Technology Co., Ltd., Beijing, China. Her research interests include wind turbine design and power system integration.

**Xiangqian Liu** received the Ph.D. degree in control theory and control engineering from Tsinghua University, Beijing, China, in 2000. He is currently with the School of Computer and Information Technology, Beijing Jiaotong University, Beijing, China. His research interests include advanced operation control system and optimal control.